Advanced Functional Materials

ADVANCED FUNCTIONAL MATERIALS
www.afm-journal.de

RESEARCH ARTICLE OPEN ACCESS

Role of Intrinsic Electron Trapping in Negative Charging of Amorphous Alumina

Jack W. Strand[1,2,3] | Kaja H. Hiorth[4,5] | David Gao[1,2,4] | Valeri Afanas'ev[6,7] | Jaakko Akola[4,8] | Alexander L. Shluger[3,9]

[1]Nanolayers Research Computing, London, UK | [2]Nanolayers OÜ, Tallinn, Estonia | [3]Department of Physics and Astronomy, University College London, London, UK | [4]Department of Physics, Norwegian University of Science and Technology (NTNU), Trondheim, Norway | [5]Department of Applied Physics, Aalto University, Helsinki, Finland | [6]Department of Physics and Astronomy, KU Leuven, Leuven, Belgium | [7]imec, Leuven, Belgium | [8]Computational Physics Laboratory, Tampere University, Tampere, Finland | [9]WPI-Advanced Institute for Materials Research (WPI-AIMR), Tohoku University, Sendai, Japan

Correspondence: Jack W. Strand (jack.strand.14@ucl.ac.uk)

Received: 9 October 2025 | **Revised:** 15 February 2026 | **Accepted:** 2 June 2026

Keywords: amorphous oxides | dft calculations | electron trapping | high-k oxide

ABSTRACT

Negative charging of amorphous alumina (a-Al_2O_3) films is important for many applications, but its nature is not yet fully understood. We investigate whether intrinsic electron traps in a-Al_2O_3 can contribute to film charging before and after high-temperature anneal. Amorphous and partially crystallized alumina models are created using the melt-quench approach. Analysis of a large set of models covering a wide range of film densities using hybrid density functional theory shows both spontaneous and activated trapping of electrons in a-Al_2O_3. Spontaneous trapping is found to be more prominent in high-density, partly crystallized, models. Two types of traps are found: single-center traps and two-center traps. In the single-center case, electrons localize on five-coordinated Al ions in tetragonal pyramid coordination. Two-center traps have electron states shared between close Al-Al pairs. The optical ionization energies of these traps are in the range of 1–4 eV. We discuss these findings in the context of exhaustive photo-depopulation spectroscopy (EPDS) measurements of trapped electrons in as-deposited and partially crystallized a-Al_2O_3 films.

1 | Introduction

Amorphous oxide films play an important role in many technologies as dielectrics in field effect transistors and memories (SiO_2, HfO_2, Al_2O_3, for example) and semiconductors (indium gallium zinc oxide (IGZO), Ga_2O_3, and others) in thin-film transistors [1–4]. Their performance in devices is affected by various degradation effects attributed to pre-existing and generated defects. Such defects can trap carriers [5, 6], leading to oxide charging, which can be detrimental to device performance, for example, through phenomena such as threshold voltage shift in complementary Metal-Oxide-Semiconductor (CMOS) devices. Therefore, studies of oxide defects and their possible charge states are important for developing new technology and improving the reliability of devices. Although there is a large number of experimental investigations into the charging of oxide films, atomistic simulations are often required to assist the interpretation of the experimental data and identify defects responsible for charging.

In particular, it is well established that the films of amorphous aluminium oxide Al_2O_3 (a-Al_2O_3) grown using different deposition techniques contain a significant density of negative charges [7–12]. Understanding electron trapping in a-Al_2O_3 films is important in the development of charge trap flash memory cells [11, 12] and amorphous Indium Gallium Zinc Oxide (a-IGZO) transistors [13], as well as in understanding the combustion mechanisms of aluminised solid fuels [14]. Furthermore, in some applications, the presence of charge is desirable. For example,

a-Al_2O_3 layers in silicon solar cells are often used for electrostatic surface passivation, and their charging behavior is a key factor in cell performance [15–17] by introducing substantial band bending at the silicon side of the Si/a-Al_2O_3 interface.

The formation of negative charges in alumina can result from electron transfer from Si to deep electron traps inside the oxide. A wide variety of models for electron traps have been introduced, ranging from interstitial oxygen [18] to oxygen vacancies [19] and aluminium vacancies [15], as discussed in ref. [20]. Negative charging of amorphous oxide films can also be caused by electron trapping at intrinsic sites in the amorphous network, as predicted in amorphous SiO_2, HfO_2, and TiO_2 [5]. However, the conduction band minimum (CBM) of crystalline alumina has a high dispersion (see e.g., [21]) that prevents the formation of electron polarons. Initial attempts to investigate intrinsic electron trapping in a-Al_2O_3 proved unsuccessful, and it has been concluded that there is no electron trapping in a-Al_2O_3 [22]. However, later studies have shown that electrons can be trapped at a small number of Al sites in a-Al_2O_3 [23] and this can facilitate the formation of oxygen vacancy - oxygen interstitial pairs contributing to the dielectric breakdown of a-Al_2O_3. These studies have shown that it remains challenging to identify intrinsic electron trapping sites in a-Al_2O_3 and other amorphous oxides. In materials where such trapping has been predicted, such as SiO_2 [24], HfO_2 [25], TiO_2 [26], $Ge_2Sb_2Te_5$ [27], and Al_2O_3 [23], these electron traps can accommodate two electrons, making them invisible to ESR.

Therefore, theoretical modeling remains one of the main direct methods of studying the atomic nature of these traps.

In this work, we discuss the challenges in modelling these electron states in amorphous oxides and further develop models of intrinsic electron trapping in a-Al_2O_3 using DFT simulations. In particular, we investigate whether spontaneous electron trapping is possible in a-Al_2O_3. We find a number of structural motifs in the amorphous structures, which facilitate trapping of electrons from the conduction band into highly-localized trap states, which may contribute to negative charging. We discuss how these findings can help to understand the results of exhaustive photodepopulation spectroscopy (EPDS) measurements of trapped electrons in as-deposited and partially crystallized a-Al_2O_3 films presented in the next section.

2 | Experimental Background

The structural identification of the electron trapping sites in a-Al_2O_3 is hampered by the absence of electron spin resonance signals associated with these electron states [15, 18, 28–32]. In this context, EPDS has proven to be a very efficient and accurate tool for the analysis of the energies of electron trapping sites in thin oxide films, including a-Al_2O_3 [11]. EPDS measures the energy levels of the defects by monitoring the density of electronic charge remaining in the film after the photo-excitation of electrons into the conduction band [11, 33, 34]. Based on the principles of internal photoemission spectroscopy, it has provided the trap density at various depths in a wide variety of oxide films [35].

In this section, we recap the results of previous EPDS measurements on Al_2O_3 and HfO_2 films. Figure 1 compares the energy

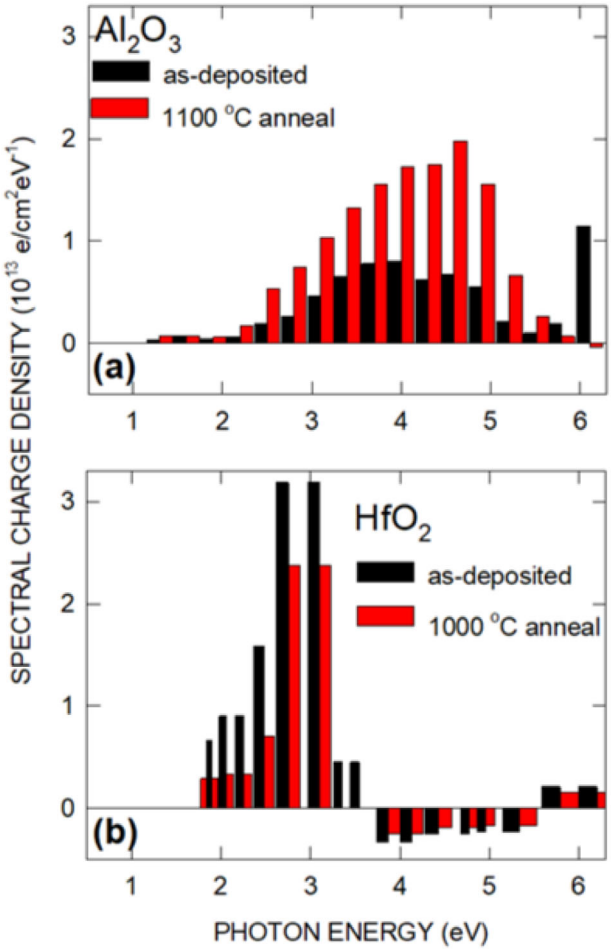

FIGURE 1 | Density of trapped electrons per unit area released upon illumination with monochromatic light with stepwise increase of the photon energy and normalized to the energy size of the increment. The results are shown for ALD-grown 20 nm Al_2O_3 (a) and 19 nm HfO_2 (b) layers in the as-deposited state and after high-temperature crystallization anneal in N_2 ambient at the indicated temperatures.

distributions of trapped electrons emitted from the trapping sites by optical excitation in Al_2O_3 (a) and HfO_2 (b) layers deposited on top of tunneling SiO_2 layer (4–5 nm thick) thermally grown on (100)Si substrate [11, 36, 37]. In both cases deep traps, in the range 2 – 3.5 eV are observed. We note that detection of deep traps in HfO_2 is hampered by electron photoemission from the silicon valence band (VB) into the conduction band (CB) of tunnel SiO_2 resulting in compensating electron trapping in the high-k oxide at photon energies approaching 4 eV. This results in negative charging seen in Figure 1b [37].

However, the most remarkable difference between electron trapping in Al_2O_3 and HfO_2 is observed after high-temperature annealing in N_2 atmosphere, which leads to partial crystallization of oxide films (see, for example, ref. [38]). In the case of HfO_2, the density of trapped electrons decreases after anneal. In contrast, the crystallization of alumina into cubic γ-phase results in significant increase of electron trapping. The high density of trapped electrons in Al_2O_3 in combination with lower dielectric permittivity than in HfO_2 induces a retarding electric field sufficient to block electron photo-injection from Si substrate. As

a result, the trapped electron energy distribution can be studied over a wider range of energies below the Al_2O_3 conduction band minimum (CBM). It should be mentioned that the position of the CBM is shifted upward by 0.5 eV upon full crystallization due to the bandgap widening in γ-Al_2O_3 [39, 40], which can result in a shift in the position of the levels of electron traps with respect to those found in the amorphous phase.

In the following, we discuss whether the formation of single- and two-electron traps in a-Al_2O_3 can contribute to the spectra in Figure 1(a) and explain the difference with a-HfO_2 upon anneal.

3 | Methodology

3.1 | DFT Calculations

We use DFT implemented in the CP2K Quickstep code [41]. CP2K uses a primary linear combination of atomic orbitals (LCAO) basis set with an auxilliary planewave basis set. The Goedecker-Teter-Hutter (GTH) pseudopotentials and basis sets are used [42, 43], which use a molecularly-optimized double-ζ basis for the valence electrons in all cases, with higher l orbitals used for polarisation basis functions. An auxiliary planewave basis set with a cutoff of 7875 eV is used. Due to computer time limitations, all calculations with an even number of electrons are non spin-polarized performed in the singlet spin state.

The hybrid functional PBE0-TC-LRC [44] is used to calculate exchange-correlation (XC) energy. The parameters of this functional were tuned to enforce the piecewise linearity with respect to fractional particle occupations. This parametrization has previously been used to predict the properties of trapped holes in a-Al_2O_3 [45]. Hybrid XC functionals use a non-local operator to calculate the exchange energy, which is very computationally expensive. Therefore, we use the auxiliary density matrix method (ADMM) [46] to improve the efficiency of our calculations, allowing us to study systems containing several hundred atoms. All calculations are performed at the Γ point. In the calculation of the defect charge transition levels, we used the charge correction method from reference [47]. In no case does the total correction exceed 0.2 eV.

Analysis of the electronic structure is assisted by calculating the inverse participation ratio (IPR) of the Kohn-Sham (KS) states. The IPR exploits the atom-centered basis to give a measure of localization of the KS states. If the KS orbitals are written as $\psi_n = \sum_{i=1}^{N} a_{ni}\phi_i$, then the IPR is defined as

$$\mathrm{IPR}(\psi_n) = \frac{\sum_{i=1}^{N} a_{ni}^4}{\left(\sum_{i=1}^{N} a_{ni}^2\right)^2} \quad (1)$$

The IPR takes a value from 0 to 1, where zero means that the state is completely delocalized.

3.2 | Modelling of Amorphous Structures

In previous calculations, we used ten a-Al_2O_3 periodic cells containing 360 atoms produced using the melt-and-quench (M&Q) method in the NPT ensemble and the modified Matsui interatomic potential [48]. This potential has shown good results in modeling liquid and amorphous alumina, as discussed recently in ref. [49]. The geometries of the generated structures were further optimized using DFT and are described in detail in ref. [22]. In ref. [22], however, the models had cell parameters optimized in PBE and atomic positions optimized with the PBE0-TC-LRC functional. In this work, we have fully optimized both the cell parameters and atomic positions of the models using the PBE0-TC-LRC functional. This leads to an increase in the average density of these models compared to ref. [22], from 3.14 gcm^{-3} to 3.26 gcm^{-3}, but without change in the distributions of the coordinate numbers. This density as well as the distribution of coordination numbers agree well with the experimental data for the ALD grown films and modeling of a-Al_2O_3 samples presented in ref. [50].

The concentration of electron trapping sites in a-Al_2O_3 is lower compared to amorphous HfO_2 where a few electron trapping sites were detected in each periodic cell [25]. Therefore, a much larger ensemble of amorphous structures is needed for more reliable predictions. In this work, we extended this ensemble by including 100 amorphous periodic cells containing 300 atoms created using the same M&Q procedure and a classical force field [48], as described in detail in ref. [22] (Figure 2a). In amorphous structures, the distributions of coordination numbers change substantially with respect to crystal phases. For example, in corundum, all Al ions are six-coordinated ($^{[6]}$Al). However, in our amorphous Al_2O_3 models, only 3% are $^{[6]}$Al, with most (55 %) being $^{[4]}$Al, in agreement with [50] (see also discussion in ref. [51]).

3.3 | Modelling Electron Trapping

It is well established that electron localization to form a polaron in a crystal can require overcoming an energy barrier [52]. In static DFT calculations, an extra electron added to a periodic cell is initially delocalized at CBM. Finding a localized solution for this electron in a perfect crystal requires mimicking the lattice distortion to initiate the electron localization in a particular lattice region and break the crystal symmetry [53, 54], (a 'bond distortion' method) accompanied by full lattice relaxation.

The computational procedure in the amorphous phase is similar; however, electrons and holes often localize without initial bond distortions because the structural disorder breaks the symmetry and can create the so-called "precursor" sites for electron or hole trapping. Such sites can be identified by analyzing the character of the localization of electronic states calculated using the IPR method. The results of IPR calculations given in ref. [22] show that there are no localized states at the CBM of a-Al_2O_3 structures described there. However, some degree of localization is found in several structures of a-Al_2O_3 studied in this work, as discussed in detail below. If an extra electron is localized without any initial bond distortion, we refer to this as "spontaneous" because it is barrier free. However, in some cases, a localized state can only be found after bond distortions are induced, and without such distortions the electron remains in a delocalized state at the CBM. This suggests the presence of an energy barrier between the delocalized and localized states. We call this trapping "activated".

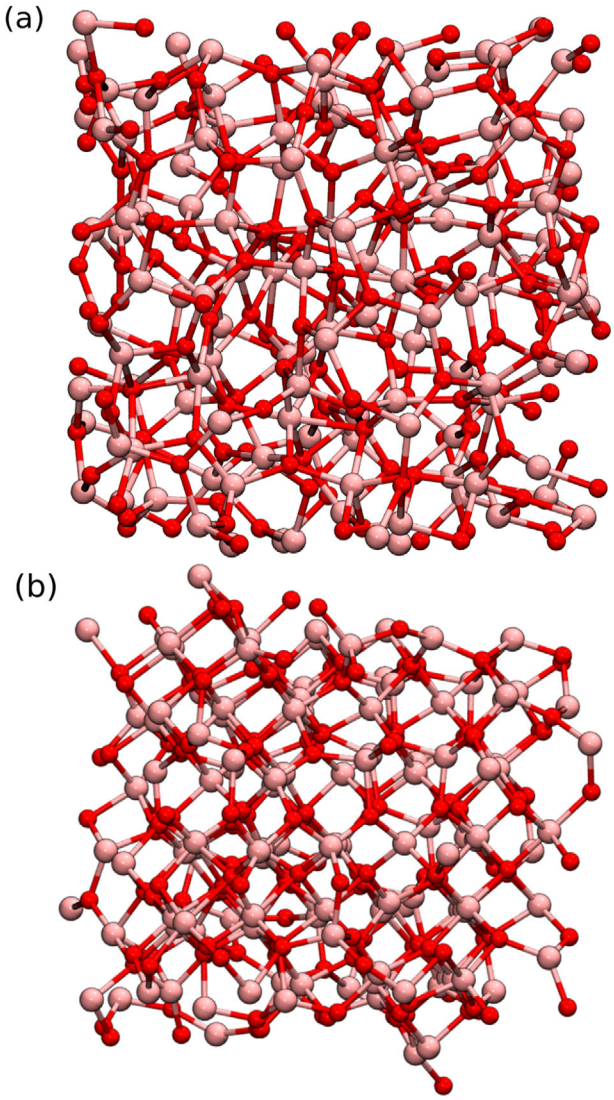

FIGURE 2 | (a) Ball-and-stick structure of a unit cell of one of the low-density a-Al_2O_3 periodic cells. (b) Ball-and-stick structure of a unit cell of a high-density Al_2O_3 model. The density of the model shown is 3.47 gcm^{-3}. The model has a higher amount of crystallinity, however, disorder is still clearly observable in the system. Peach balls indicate Al ions, read balls indicate O ions.

To characterize the thermal stability of the electron traps, we calculate the trapping energy as:

$$E_t = E_{CBM} - E_{trap} \quad (2)$$

where E_{CBM} is the total energy of the -1 charged system with an electron in the CBM, and E_{trap} is the total energy of the relaxed system with an electron localized into a trap state. A positive trapping energy indicates a thermodynamically favorable trapping. The trapping energy is equivalent to the polaron thermal ionization energy. However, calculations of energy barriers for polaron trapping are quite challenging due to the non-adiabatic character of transformation between delocalized and strongly localized states (see e.g., discussion in ref. [55]).

Amorphous structures have large variations in morphology and local environment. Such variations can affect properties of interest, and this leads to the need to sample many different morphologies and calculate statistical properties such as mean averages and standard deviations. All 110 structures, which span a wide range of densities, were investigated for the existence of spontaneous electron trapping.

In the case of activated trapping in amorphous structures, sites that are amenable to electron trapping are unknown and finding them is a daunting task. To choose which initial distortions to apply, we turn to the previous literature on the topic. In these studies [5, 6, 24, 25], trapping sites are often characterized by features such as extended cation–anion bonds and atypical coordination numbers. For example, an electron may be expected to trap on a low-coordination Al ion, as the lower number of nearby anions will result in a lowering of the electrostatic potential (as seen by the electron). Therefore, to try and find electron traps, we focus mainly on four-coordinated ($^{[4]}$Al) ions. In addition, we extend Al-O bonds by approximately 0.1 Å, and also displaced Al ions toward each other by approximately 0.1 Å in multiple locations in amorphous structures. The choice of 0.1 Å corresponds to the bulk vibrational amplitude of 0.12 Å at room temperature, as suggested in ref. [56]. The system's geometry is fully optimized following these initial displacements to find stable structures. We also attempted a second type of distortion, where O-Al-O bonds were widened. However, in no case did we successfully find a stable non-spontaneous trap using this perturbation. Because these calculations require large computational resources they were carried out only for ten structures described in ref. [22], which are completely disordered and have lower densities.

4 | Results of Calculations

4.1 | Spontaneous Electron Trapping

The set of models produced using the melt-quench spans densities from 3.10 to 3.67 gcm^{-3}, with an average density of 3.23 gcm^{-3}. We note that the range of alumina densities studied in our work corresponds well to the experimental values indicating the increase of the film density from 3.0–3.2 gcm^{-3} for the as-deposited ALD alumina [57] to ≈3.7 gcm^{-3} (0.93 of the bulk sapphire density) reported in ref. [58] upon annealing at 950°C. Two of these models are shown in Figure 2. The average KS bandgap of the models is 5.6 eV. The concentration of aluminium ions with different coordination with respect to oxygen ions, averaged in all 110 structures, is $^{[4]}$Al = 55.2%, $^{[5]}$Al = 32.9% and $^{[6]}$Al = 11.9%. The highest-density models show signs of crystallization as indicated by high-coordinated aluminium. One such model is shown in Figure 2b, where the coordination number distribution of Al ions with respect to O ions is: $^{[4]}$Al = 30.8%, $^{[5]}$Al = 20.8% and $^{[6]}$Al = 48.3%. High concentrations of $^{[6]}$Al are indicative of the crystal phases of alumina, for example corundum, in which all Al ions are six coordinated. In the highest density model, 73% of the Al ions are six coordinated with respect to oxygen.

Figure 3 shows the IPR spectrum of a typical amorphous Al_2O_2 model. The conduction band states are delocalized, as illustrated

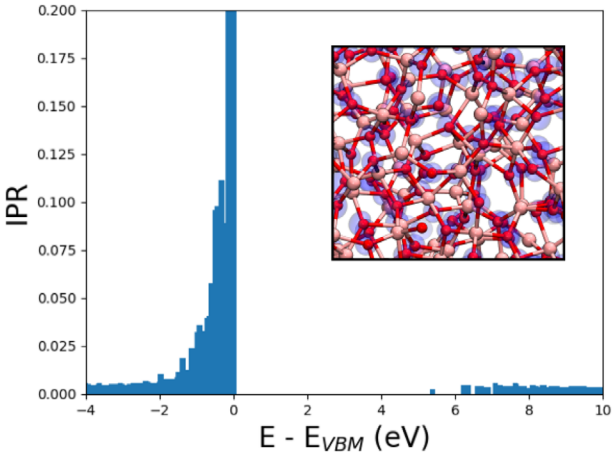

FIGURE 3 | IPR of a typical a-Al_2O_3 model without spontaneous electron trapping. The VB edge states are part-localized, whereas the CB edge states are delocalized, similar to those in the crystal. Inset: Shows the CBM state (blue surfaces) in the bulk a-Al_2O_3 model.

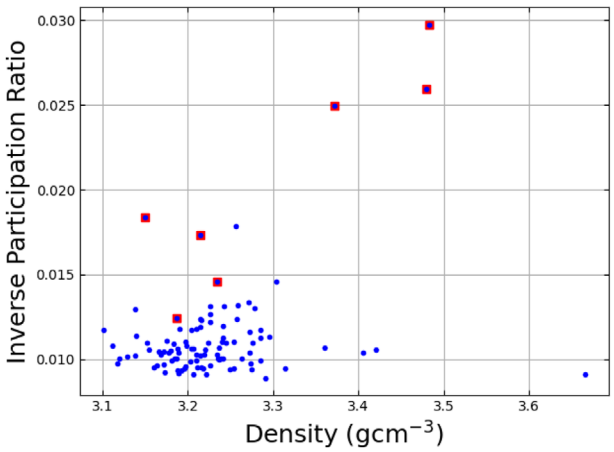

FIGURE 4 | Correlation between densities of 100 amorphous structures and IPR values or degree of localization of the CBM state. Data points highlighted with a red square are those found to have spontaneous electron traps. In total seven structures out of 100 can trap an electron. The structure with the largest IPR value of the CBM state contains two unique electron traps.

in the inset of Figure 3. The valence band has states localized at the edge, with a gradual transition to delocalized states at approximately 1 eV below the valence band edge. This localization of states near the valence band edge is common in amorphous oxides and has been reported in other materials [26, 59, 60]. It has been linked to the formation of deep, intrinsically trapped holes that are predicted to be stable at room temperature. The lack of localization in the conduction band is conducive to the fact that most of the a-Al_2O_3 models analyzed do not contain spontaneous traps.

We do, however, see a degree of localization of KS states at the CBM in some models. Figure 4 shows a correlation between the densities of the 100 amorphous alumina structures and the IPR of the CBM before extra electrons have been introduced. Structures capable of trapping an electron tend to have a CBM state with a larger IPR value, indicating partial localization of the electron states even before ions have been displaced via the polaronic formation mechanism.

Upon injecting extra electrons and geometry optimization we find that electrons trap spontaneously in seven of the 100 amorphous alumina structures (indicated in Figure 4), one of which contains two unique traps. The electrons localize strongly near either one Al (single-center, Figure 5a) or between two Al atoms (bond-like, Figure 5b), resulting in a significant increase in the spin density around the Al atom(s) and an in-gap KS energy eigenvalue. The single-center traps tend to be five-coordinated $^{[5]}$Al with close to 90 and 180 degree bond angles exposing an open face where the electron can localize. That is, the Al polyhedron is a distorted square pyramidal structure (Figure 5a; and Figure 6b).

In the case of the bond-like configurations, there is significant displacement of Al ions toward one another. On average, the Al-Al distance is reduced by 0.45 Å, forming a dimer with an average distance of 3.2 Å. The trapping energies range from 0.5 to 1.1 eV. These are similar to trapping energies found in previous studies in amorphous oxides [5], and the depth suggests that the traps will be stable at room temperature. Although the electron-trapping structures have a wide range of densities, the distribution is skewed, with nearly half of the electron traps found in higher-density models with larger IPR values. Analysis of the structures shows that the traps here have a distorted square pyramidal structure. The KS levels of the traps range from 1.7 to 3.0 eV below the CBM.

The fact that three (nearly half) of the spontaneous traps appear in the higher density models demonstrates the importance of morphology to electron trapping. In real amorphous films, the lower-density structures may correspond to as-deposited amorphous thin films, for example, which tend to show higher degrees of disorder. The higher-density structures may correspond to annealed films, which tend to show a more complex morphology with a higher degree of crystallinity [39]. Therefore, we suggest that as-deposited, highly disordered films have traps which are bond-like in nature, whereas part-crystalline films have more single-center intrinsic traps which can localize electrons barrier-free. For the case of low-density amorphous films, we are able to make an estimate of the trap density based on the frequency of spontaneous trapping sites we have observed in our models. In total, four of the low-density amorphous Al_2O_3 models show spontaneous trapping. This means precursors to spontaneous trapping have a density of 0.9×10^{-19}cm^{-3}. We cannot reliably estimate the trap density in the high-density polycrystalline models because in this case it depends sensitively on the degree of crystallinity of a given film and its grain boundary density. Such morphological properties will strongly depend on the film fabrication technique and conditions, implying that a general precursor concentration does not exist.

4.2 | Activated Electron Trapping

In all other structures considered, an initial perturbation is required to find the localized state. Without this perturbation, an extra electron is delocalized across all of Al ions, as shown in the inset in Figure 3. Applying distortions to ten unit cells of a-Al_2O_3 with lower densities, we find a total of 6 sites where

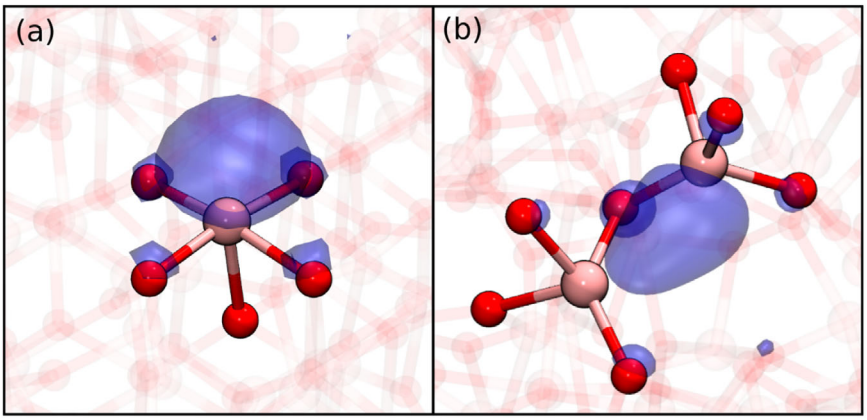

FIGURE 5 | (a) A single center electron trap state in a-Al_2O_3. Peach spheres indicate Al ions and red spheres indicate oxygen. The blue surface is a representative iso-surface of the spin density of the trapped electron. (b) A two-center (bond-like) intrinsic electron trap in a-Al_2O_3.

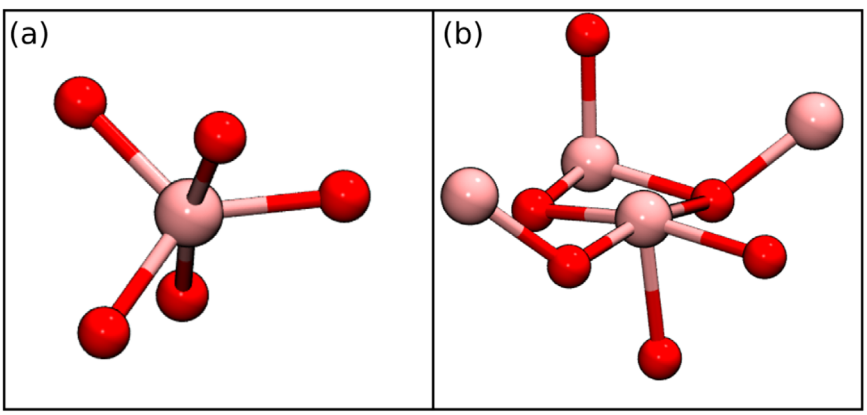

FIGURE 6 | (a) A typical $^{[5]}$Al ion from an a-Al_2O_3 model which does not have spontaneous electron trapping. (b) A $^{[5]}$Al ion which acts as a precursor to spontaneous trapping.

stable intrinsic traps can form, giving a density of 1.6×10^{20} cm^{-3}. It is likely that this forms a lower bound for the concentration of potential trapping sites, since it is possible that more activated traps exist which we have not yet found. However, full occupations of all potential trapping sites may not be achievable, as the Coulomb repulsion between traps may limit the total trap density. All but one intrinsic trap configuration have "bond-like" configurations, where electron density is shared between two adjacent Al ions (Figure 5b), and the two Al ions move toward each other with an average displacement of 0.3 Å. The two ions involved are mostly $^{[4]}$Al, and the electron trap is similar to the Al–Al bond defect found in the oxygen deficient a-Al_2O_3 structure in ref. [51] where electrons are shared between neighboring $^{[3]}$Al ions. Also, the two Al ions share either a single or no O ion between them - in no case did we identify a trap existing on adjacent Al ions sharing two O ions. An alternative description is that the trap occurs between either corner-sharing polyhedra, or between unconnected but adjacent Al polyhedra, but never between edge-sharing Al polyhedra. Across all of the bond-like trap configurations, the Al-O bonds are stretched by 0.06 Å, on average. The main relaxation comes from the movement of the Al–Al pair, which displace toward one another by, on average, 0.3 Å. In one case, a single-center trap configuration is found, with the electron localized on a five-coordinated Al ion in the polyhedron with a distorted square pyramidal structure. This configuration is similar to the spontaneous single center traps (Figure 6a).

The average trapping energy of the activated traps is 0.3 eV, ranging from 0.0 to 0.7 eV. In general, it is seen that the electron traps with shorter Al–Al distances are deeper. This can be understood as follows: A closer Al–Al distance will produce a deeper potential well into which the electron can localize. However, displacing Al ions costs energy as it deforms the network. Therefore, traps on a short-separation Al–Al pair can achieve a more favorable configuration without paying too much energy to distort the lattice and bring Al ions close together. The KS eigenvalues for the activated traps spread from 1.7 to 2.4 eV below the CBM, covering a range roughly similar to that of the spontaneous electron traps.

We note that activated electron trapping should be possible in some other amorphous models of our ensemble. However, identifying such traps and calculating the activation barriers for electron trapping require extensive computational resources and are beyond the scope of this study.

Since the trapping of these configurations are thermally activated, the rate of trapping is determined by the energetic barrier. The four calculated barriers for the activated trapping process are very low (near 0.1 eV). However, we could not converge the barrier calculations in all cases considered due to the breaking of the adiabatic approximation.

4.3 | Creation of Two-Electron Traps

All single-electron trap models were found to be capable of trapping a second electron in a -2 charge state of the system. Traps with two extra electrons are also called bipolarons in previous studies [5]. We define a second electron trapping energy as:

$$E_{2t} = (E_{CBM} + E_{trap}) - (E_{bulk} + E_{double\text{-}trap}) \quad (3)$$

where E_{CBM} is the energy of the CBM, E_{trap} is the energy of the single-electron trap, E_{bulk} is the energy of the amorphous cell, and $E_{double\text{-}trap}$ is the energy of the trap with two electrons. E_{2t} is equivalent to the thermal ionization energy of one electron into the CBM.

In the case of spontaneous traps, the range of trapping energies for the second electron is from 0.3 to 1.3 eV, averaging 0.8 eV. The wider range of values compared to the single trapping energies reflects the fact that some of the electrons trap more deeply than the first and some less deeply. In all cases, the second electron is trapped onto the same Al ion as the first, though the distribution is altered slightly with the electron KS state being more shared with some neighboring Al ions.

The activated electron trap models can all trap a second electron to form a -2 trap state. In all cases the second electron traps spontaneously, that is, no additional perturbation is required to initiate localisation of the second electron. In all cases, the trapping of two electrons creates a deeper electronic state than that of one. The average trapping energy of the second electron is 0.9 eV, ranging from approximately 0.5 eV up to 1.7 eV. Electron trapping distorts the surrounding structure, causing atomic displacements of 0.1 to 0.2 Å of the nearest neighbour ions.

We also find an interesting case of a single-center trap in the -1 charge state with a relatively low trapping energy for the first electron (0.1 eV) converting into the Al–Al bond trap upon trapping the second electron with a much larger second trapping energy of 1.74 eV. This is caused by the significant relaxation on a nearby Al ion, which moved toward the electron trap and created a shorter Al–Al bond, transforming the single-center trap into the bond-like configuration seen in the other five models. In addition, the local atomic reorganization is large enough so that a $^{[4]}$Al ion transforms into a $^{[3]}$Al ion. This makes this configuration very similar to Al–Al bonds found in oxygen defficient a-Al_2O_3 in ref. [51].

5 | Discussion and Conclusions

We have simulated electron trapping in a set of stoichiometric a-Al_3O_3 models using hybrid DFT. Similar to other amorphous oxides, electrons can trap in a-Al_2O_3 intrinsically, that is, without oxygen deficiency or impurities.

Analysis of a large set of models covering a wide range of densities shows spontaneous and activated trapping of electrons in a-Al_3O_3. Spontaneous trapping is found to be more prominent in high-density, partly crystallized, models. Two types of traps are found - single-center and two-center traps.

In the single-center case, electrons localize on $^{[5]}$Al ions with large O–Al–O angles forming a tetragonal pyramid coordination shown in Figure 6b exposing these Al ions to electron trapping. Such structures are abundant on surfaces of γ-alumina [61] and inside grain boundaries in alumina [62, 63]. However, most $^{[5]}$Al ions in amorphous Al_2O_3 are not of this type, but instead have narrower and more equal O-Al-O angles, resulting in O ions shielding the Al ion more evenly (Figure 6a).

In the case of two-center traps, there is localization around $^{[3]}$Al or $^{[4]}$Al ions and a sharing of electron density between the $^{[4]}$Al ions in a bond-like fashion.

Thus, the Al–Al pairing seems to be a fairly general feature of localized electron states in alumina, as was found in the previous work [51]. Similar metal-metal bonding has been predicted in other systems [64], suggesting this as a defect motif not limited to just Al_2O_3. We have also investigated the activated trapping of electrons in alumina and found bond-like traps that can form in amorphous alumina as a result of thermal fluctuations and have lower trapping energies. Our results suggest that spontaneous trapping is more probable in partially crystallized samples; however, our sampling is insufficient for more accurate predictions.

In the following, we discuss how these findings help us to resolve the apparent difference in the behavior of a-HfO_2 and a-Al_3O_3 after the high temperature anneal shown in Figure 1.

Density Functional Theory (DFT) simulations have explained the EPDS spectra in a-HfO_2 shown in Figure 1b by the formation of two kinds of deep electron traps energetically distributed at around 2.0 and 3.0 eV below the oxide conduction band and attributed to single and bi-polaron electron states, respectively [37]. The reduction in the number of states that contribute to the EPDS spectrum of a-HfO_2 is consistent with the decrease in the volume of the film occupied by amorphous or disordered hafnia where electrons are trapped in deep polaron-like states [6]. These data also suggest that anneal does not cause full crystallization of HfO_2 as polarons in crystalline samples have much lower trapping energies [25, 53] absent in Figure 1b.

On the other hand, the calculations in ref. [20] have shown that the results for a-Al_2O_3 in Figure 1a can be understood assuming that negatively charged oxygen interstitials, O_i, and Al vacancies, V_{Al} in as-prepared samples are nearly compensated for by positively charged H_i, V_O, and Al_i defects. Following electron injection, the deep states of Al_i, V_O, and H_i in the bandgap become occupied by electrons, and the sample becomes negatively charged. The optical ionization energies of these states into the oxide conduction band are consistent with the results of EPDS measurements [20].

The results of ref. [65] allow us to directly link the electron trapping energies found in this work to the optical excitation energies measured in EPDS. Assuming similar behavior of the electron traps in amorphous HfO_2 and Al_2O_3, we can apply the ratio between optical and thermal electron emission energies of 2.2 found there. The resulting energies are consistent with the presence of the low-energy tail at 1.2 – 2.2 eV in Figure 1a, which can be attributed to single- and two-electron traps. Some of the two-electron states can also contribute in the energy range of 2 – 4 eV. However, these results cannot fully explain the significant increase in intensity in the EPDS spectra in the energy range of 4–5 eV seen in Figure 1a after the anneal.

An additional source of negative charge could stem from the grain boundaries in polycrystalline alumina films formed as a result of anneal. They have been shown to contain a high concentration of $^{[5]}$Al ions in tetragonal pyramid coordination [62, 63] structurally analogous to the electron traps found in the bulk. Assuming that they are capable of trapping electrons, these states can contribute to negative charging after annealing. The high electron density localization at these sites has been shown in ref. [63], however, electron trapping at these sites requires further studies. We note that a similar effect should occur in polycrystalline hafnia. However, amorphous hafnia has a much higher concentration of deep intrinsic electron trapping sites, which vanish after crystallization and are replaced by a lower number of under-coordinated Hf sites at grain boundaries (see also discussion in ref. [66]). If this hypothesis is correct, the electronic properties of electron traps can be used as indicators of degree of crystallinity of amorphous films.

Another possibility is that high-temperature annealing causes changes in the chemical composition of alumina through reactions at the interface. For example, it has previously been suggested that the interstitial O near the interface of Al_2O_3 with SiO_2/Si substrate contributes to to the fixed negative charge [67]. Oxygen vacancies can form inside a-Al_2O_3 film as a result of reactions with SiO molecules that form at the Si/SiO_2 interface during annealing in the N_2 atmosphere at 1100°C [68, 69].

In summary, our results show that electrons can trap in deep states intrinsic to amorphous alumina structures and that the character of trapping and trapping energies depend on the degree of crystallinity of initially amorphous films. However, these findings cannot fully explain the observed increase in the number of deep electron traps occurring after high-temperature annealing. These results are consistent with the fact that the defect characteristics in deposited amorphous oxide films depend on the film properties and deposition techniques. These insights into electron trapping in oxides improve our understanding of the mechanisms of negative charging of oxide films in applications and their role in the reliability of future nanoscale devices. In particular, the results of previous works show that the formation of two-electron traps can faciliate the formation of O vacancies and contribute to oxide degradation and dielectric breakdown [23, 70, 71]. These results can be useful for understanding the electronic component of the mechanism responsible for atomic rearrangements and crystallization of amorphous Al_2O_3 films under irradiation [72–74].

Acknowledgements

J.S. and A.S. acknowledge support from the EPSRC grant EP/R034540/1 and the computer resources provided by ARCHER2 UK National Supercomputing Service (http://www.archer2.ac.uk) via the membership of the UK's HEC Materials Chemistry Consortium funded by EPSRC (EP/X035859). This work is supported by the Chips JU project ARCTIC (Project #101139908). The project is supported by the Chips Joint Undertaking and its members (including top-up funding by Belgium, Austria, Germany, Estonia, Finland, France, Ireland, The Netherlands and Sweden). ARCTIC gratefully acknowledges the support of the Canadian and the Swiss federal governments. K.H. and J.A. acknowledge supercomputing resources at CSC - IT center for Science (Finland) and Sigma2 - the National Infrastructure for High Performance Computing and Data Storage in Norway (project NN9497K).

Conflicts of Interest

The authors declare no conflicts of interest.

Data Availability Statement

The data that support the findings of this study are available from the corresponding author upon reasonable request.

References

1. J. Robertson and R. M. Wallace, "High-k Materials and Metal Gates for CMOS Applications," *Materials Science and Engineering: R: Reports* 88 (2015): 1–41.

2. S. Y. Lee, "Comprehensive Review on Amorphous Oxide Semiconductor Thin Film Transistor," *Transactions on Electrical and Electronic Materials* 21 (2020): 235–248.

3. B. Wang, W. Huang, L. Chi, M. Al-Hashimi, T. J. Marks, and A. Facchetti, "High-k Gate Dielectrics for Emerging Flexible and Stretchable Electronics," *Chemical Reviews* 118, no. 11 (2018): 5690–5754.

4. J. E. Medvedeva, D. B. Buchholz, and R. P. Chang, "Recent Advances in Understanding the Structure and Properties of Amorphous Oxide Semiconductors," *Advanced Electronic Materials* 3, no. 9 (2017): 1700082.

5. J. Strand, M. Kaviani, V. V. Afanas'ev, J. G. Lisoni, and A. L. Shluger, "Intrinsic Electron Trapping in Amorphous Oxide," *Nanotechnology* 29, no. 12 (2018): 125703.

6. J. Strand, M. Kaviani, D. Gao, A.-M. El-Sayed, V. V. Afanas'ev, and S. A. L., "Intrinsic Charge Trapping in Amorphous Oxide Films: Status and Challenges," *Journal of Physics: Condensed Matter* 30, no. 2 (2018): 233001.

7. V. V. Afanas'ev and A. Stesmans, "Stable Trapping of Electrons and Holes in Deposited Insulating Oxides: Al_2O_3, ZrO_2, and HfO_2," *Journal of Applied Physics* 95, no. 5 (2004): 2518–2526.

8. B. Govoreanu, D. Wellekens, L. Haspeslagh, J. De Vos, and J. Van Houdt, "Investigation of the Low-Field Leakage Through High-k Interpoly Dielectric Stacks and Its Impact on Nonvolatile Memory Data Retention," *Technical Digest of the International Electron Devices Meeting (IEDM)* (2006).

9. J. J. H. Gielis, B. Hoex, M. C. M. van de Sanden, and W. M. M. Kessels, "Negative Charge and Charging Dynamics in Al_2O_3 Films on Si Characterized by Second-Harmonic Generation," *Journal of Applied Physics* 104, no. 7 (2008): 073701.

10. Y. N. Novikov, V. A. Gritsenko, and K. A. Nasyrov, "Charge Transport Mechanism in Amorphous Alumina," *Applied Physics Letters* 94, no. 22 (2009): 222904.

11. M. B. Zahid, D. R. Aguado, R. Degraeve, et al., "Applying Complementary Trap Characterization Technique to Crystalline Gamma-Phase Al_2O_3 for Improved Understanding of Nonvolatile Memory Operation and Reliability," *IEEE Transactions on Electron Devices* 57, no. 11 (2010): 2907–2916.

12. Y. Li, Y. Pei, R. Hu, et al., "Charge Trapping Memory Characteristics of Amorphous-Indium-Gallium-Zinc-Oxide Thin-Film Transistors with Defect-Engineered Alumina Dielectric," *IEEE Transactions on Electron Devices* 62, no. 4 (2015): 1184–1188.

13. K.-C. Ok, S. Oh, H.-J. Jeong, J. U. Bae, and J.-S. Park, "Effect of Alumina Buffers on the Stability of Top-Gate Amorphous InGaZnO Thin-Film Transistors on Flexible Substrates," *IEEE Electron Device Letters* 36, no. 9 (2015): 917–919.

14. A. M. Savel'ev and D. A. Yagodnikov, "Mechanism of Electric Charging of Aluminum Oxide Particles When Burning Solid Fuels," *Journal of Propulsion and Power* 38, no. 5 (2022): 771–782.

15. G. Dingemans and W. M. M. Kessels, "Status and Prospects of Al_2O_3-Based Surface Passivation Schemes for Silicon Solar Cells," *Journal of Vacuum Science & Technology A* 30 (2012): 040802.

16. B. Nemeth, S. P. Harvey, J. Li, et al., "Effect of the SiO_2 Interlayer Properties with Solid-Source Hydrogenation on Passivated Contact Performance and Surface Passivation," *Energy Procedia* 124 (2017): 295–301.

17. R. Bonilla, B. Hoex, P. Hamer, and P. Wilshaw, "Dielectric Surface Passivation for Silicon Solar Cells: A Review," *Physica Status Solidi A: Applications and Materials Science* 214, no. 7 (2017): 1700293.

18. S. Kuhnhold-Pospischil, P. Saint-Cast, M. Hofmann, et al., "A Study on Si/Al_2O_3 Paramagnetic Point Defects," *Journal of Applied Physics* 120, no. 19 (2016): 195304.

19. C. G. Van de Walle, M. Choi, J. Weber, J. Lyons, and A. Janotti, "Defects at Ge/Oxide and III-V/Oxide Interfaces," *Microelectronic Engineering* 102 (2013): 211–215.

20. O. A. Dicks, J. Cottom, A. L. Shluger, and V. V. Afanas'ev, "The Origin of Negative Charging in Amorphous Al_2O_3 Films: The Role of Native Defects," *Nanotechnology* 30, no. 20 (2019): 205201.

21. R. Santos, E. Longhinotti, V. Freire, R. Reimberg, and E. Caetano, "Elucidating the High-k Insulator αAl_2O_3 Direct/Indirect Energy Band Gap Type Through Density Functional Theory Computations," *Chemical Physics Letters* 637 (2015): 172–176.

22. O. A. Dicks and A. L. Shluger, "Theoretical Modeling of Charge Trapping in Crystalline and Amorphous Al_2O_3," *Journal of Physics: Condensed Matter* 29, no. 31 (2017): 314005.

23. P. La Torraca, A. Padovani, J. Strand, A. Shluger, and L. Larcher, "The Role of Carrier Injection in the Breakdown Mechanism of Amorphous Al_2O_3 Layers," *IEEE Electron Device Letters* 45, no. 2 (2024): 236–239.

24. A.-M. El-Sayed, M. B. Watkins, V. V. Afanas'ev, and A. L. Shluger, "Nature of Intrinsic and Extrinsic Electron Trapping in SiO_2," *Physical Review B* 89, no. 12 (2014): 125201.

25. M. Kaviani, J. Strand, V. V. Afanas'ev, and A. L. Shluger, "Deep Electron and Hole Polarons and Bipolarons in Amorphous Oxide," *Physical Review B* 94, no. 2 (2016): 020103.

26. D. Mora-Fonz, M. Kaviani, and A. L. Shluger, "Disorder-Induced Electron and Hole Trapping in Amorphous TiO_2," *Physical Review B* 102 (2020): 054205.

27. K. Konstantinou, S. R. Elliott, and J. Akola, "Inherent Electron and Hole Trapping in Amorphous Phase-Change Memory Materials: $Ge_2Sb_2Te_5$," *Journal of Materials Chemistry C* 10 (2022): 6744–6753.

28. A. Stesmans and V. Afanas'ev, "Electron Spin Resonance Observation of Si Dangling-Bond-Type Defects at the Interface of (100) Si with Ultrathin Layers of SiO_x, Al_2O_3 and ZrO_2," *Journal of Physics: Condensed Matter* 13, no. 28 (2001): L673–L680.

29. A. Stesmans and V. Afanas'ev, "Defects at the Interface of (100)Si with Ultrathin Layers of SiO_x, Al_2O_3, and ZrO_2 Probed by Electron Spin Resonance," *Journal of Vacuum Science & Technology B* 20, no. 4 (2002): 1720–1725.

30. A. Stesmans and V. Afanas'ev, "Si Dangling-Bond-Type Defects at the Interface of (100)Si with Ultrathin Layers of SiO_x, Al_2O_3, and ZrO_2," *Applied Physics Letters* 80, no. 11 (2002): 1957–1959.

31. A. Stesmans and V. Afanas'ev, "Paramagnetic Defects in Annealed Ultrathin Layers of SiO_x, Al_2O_3, and ZrO_2 on (100)Si," *Applied Physics Letters* 85, no. 17 (2004): 3792–3794.

32. A. Stesmans and V. Afanas'ev, "Interlayer-Related Paramagnetic Defects in Stacks of Ultrathin Layers of SiO_x, Al_2O_3, ZrO_2, and HfO_2 on (100)Si," *Journal of Applied Physics* 97, no. 3 (2005): 033510.

33. V. V. Afanas'ev and A. Stesmans, "Internal Photoemission at Interfaces of High-k Insulators with Semiconductors and Metals," *Journal of Applied Physics* 102 (February 2007): 081301.

34. J. Strand, M. Kaviani, V. V. Afanas'ev, J. G. Lisoni, and A. L. Shluger, "Intrinsic Electron Trapping in Amorphous Oxides," *Nanotechnology* 29 (2018): 125703.

35. V. V. Afanas'ev, *Internal Photoemission Spectroscopy: Fundamentals and Recent Advances* (Elsevier, 2014).

36. V. V. Afanas'ev, W. C. Wang, F. Cerbu, O. Madia, M. Houssa, and A. Stesmans, "Spectroscopy of Deep Gap States in High-k Insulators," *ECS Transactions* 64, no. 8 (August 2014): 17.

37. F. Cerbu, O. Madia, D. Andreev, et al., "Intrinsic Electron Traps in Atomic-Layer-Deposited HfO_2 Insulators," *Applied Physics Letters* 108, no. 22 (2016): 222901.

38. S. Jakschik, U. Schroeder, T. Hecht, M. Gutsche, H. Seidl, and J. W. Bartha, "Crystallization Behavior of Thin ALD-Al_2O_3 Films," *Thin Solid Films* 425, no. 1 (2003): 216–220.

39. V. V. Afanas'ev, A. Stesmans, B. J. Mrstik, and C. Zhao, "Impact of Annealing-Induced Compaction on Electronic Properties of Atomic-Layer-Deposited Al_2O_3," *Applied Physics Letters* 81, no. 9 (2002): 1678–1680.

40. V. V. Afanas'ev, M. Houssa, A. Stesmans, C. Merckling, T. Schram, and J. A. Kittl, "Influence of Al_2O_3 Crystallization on Band Offsets at Interfaces with Si and TiN_x," *Applied Physics Letters* 99, no. 7 (2011): 072103.

41. J. VandeVondele, M. Krack, F. Mohamed, M. Parrinello, T. Chassaing, and J. Hutter, "Quickstep: Fast and Accurate Density Functional Calculations Using a Mixed Gaussian and Plane Waves Approach," *Computer Physics Communications* 167, no. 2 (2005): 103–128.

42. S. Goedecker, M. Teter, and J. Hutter, "Separable Dual-Space Gaussian Pseudopotentials," *Physical Review B* 54, no. 3 (1996): 1703–1710.

43. J. VandeVondele and J. Hutter, "Gaussian Basis Sets for Accurate Calculations on Molecular Systems in Gas and Condensed Phases," *The Journal of Chemical Physics* 127, no. 11 (2007): 114105.

44. M. Guidon, J. Hutter, and J. VandeVondele, "Robust Periodic Hartree–Fock Exchange for Large-Scale Simulations Using Gaussian Basis Sets," *Journal of Chemical Theory and Computation* 5, no. 11 (2009): 3010–3021.

45. O. A. Dicks and A. L. Shluger, "Theoretical Modeling of Charge Trapping in Crystalline and Amorphous Al_2O_3," *Journal of Physics: Condensed Matter* 29, no. 31 (2017): 314005.

46. M. Guidon, J. Hutter, and J. VandeVondele, "Auxiliary Density Matrix Methods for Hartree–Fock Exchange Calculations," *Journal of Chemical Theory and Computation* 6, no. 8 (2010): 2348–2364.

47. T. Durrant, S. Murphy, M. Watkins, and A. Shluger, "Relation Between Image Charge and Potential Alignment Corrections for Charged Defects in Periodic Boundary Conditions," *The Journal of Chemical Physics* 149, no. 2 (2018): 024103.

48. L. Bläckberg, E. Metsanurk, A. Tamm, A. Aabloo, and M. Klintenberg, "Molecular Dynamics Study of Xenon on an Amorphous Al_2O_3 Surface," *Nuclear Instruments and Methods in Physics Research Section A: Accelerators, Spectrometers, Detectors and Associated Equipment* 759 (2014): 10–15.

49. S. Gramatte, V. Turlo, and O. Politano, "Do We Really Need Machine Learning Interatomic Potentials for Modeling Amorphous Metal Oxides? Case Study on Amorphous Alumina by Recycling an Existing Ab

Initio Database," *Modelling and Simulation in Materials Science and Engineering* 32, no. 4 (2024): 045010.

50. A. Pugliese, B. Shyam, G. M. Repa, A. H. Nguyen, A. Mehta, E. B. Webb III, L. A. Fredin, and N. C. Strandwitz, "Atomic-Layer-Deposited Aluminum Oxide Thin Films Probed with X-Ray Scattering and Compared to Molecular Dynamics and Density Functional Theory Models," *ACS Omega* 7, no. 45 (2022): 41033–41043.

51. J. Strand and A. L. Shluger, "On the Structure of Oxygen Deficient Amorphous Oxide Films," *Advanced Science* 11, no. 8 (2024): 2306243.

52. Y. Toyozawa, "Self-Trapping and Drift Motion of an Electron," *Journal of Applied Physics* 33, no. 1 (1962): 340–342.

53. D. Munoz Ramo, A. L. Shluger, J. L. Gavartin, and G. Bersuker, "Theoretical Prediction of Intrinsic Self-Trapping of Electrons and Holes in Monoclinic HfO_2," *Physical Review Letters* 99, no. 2 (2007): 155504.

54. T. D. Pham and N. A. Deskins, "Efficient Method for Modeling Polarons Using Electronic Structure Methods," *Journal of Chemical Theory and Computation* 16, no. 8 (2020): 5264–5278.

55. S. Yuan, Z. Wang, M. L. F. Baron, and K. H. Bevan, "Ab Initio Insight into the Formation of Small Polarons: A Study Across Four Metal Peroxides," *Physical Review B* 100 (2019): 205201.

56. E. A. Soares, M. A. Van Hove, C. F. Walters, and K. F. McCarty, "Structure of the $\alpha - Al_2O_3(0001)$ Surface from Low-Energy Electron Diffraction: Al Termination and Evidence for Anomalously Large Thermal Vibrations," *Physical Review B* 65 (2002): 195405.

57. B. Ilic, S. Krylov, and H. G. Craighead, "Young's Modulus and Density Measurements of Thin Atomic-Layer-Deposited Films Using Resonant Nanomechanics," *Journal of Applied Physics* 108, no. 4 (2010): 044317.

58. V. V. Afanas'ev, A. Stesmans, B. J. Mrstik, and C. Zhao, "Impact of Annealing-Induced Compaction on Electronic Properties of Atomic-Layer-Deposited Al_2O_3," *Applied Physics Letters* 81, no. 9 (2002): 1678–1680.

59. J. Strand, O. A. Dicks, M. Kaviani, and A. L. Shluger, "Hole Trapping in Amorphous HfO_2 and Al_2O_3 as a Source of Positive Charging," *Microelectronic Engineering* 178 (2017): 235–239.

60. C. Kaewmeechai, J. Strand, and A. Shluger, "Electronic Structure and Properties of Trapped Holes in Crystalline and Amorphous Ga_2O_3," *Physical Review B* 111, no. 3 (2025): 035203.

61. Z. Zhao, D. Xiao, K. Chen, et al., "Nature of Five-Coordinated Al in γ-Al_2O_3 Revealed by Ultra-High-Field Solid-State NMR," *ACS Central Science* 8, no. 6 (2022): 795–803.

62. H. Guhl, H.-S. Lee, P. Tangney, et al., "Structural and Electronic Properties of Σ7 Grain Boundaries in α-Al_2O_3," *Acta Materialia* 99 (2015): 16–28.

63. T. Yokoi, A. Hamajima, J. Wei, et al., "Atomic and Electronic Structure of Grain Boundaries in a-Al_2O_3: A Combination of Machine Learning, First-Principles Calculation and Electron Microscopy," *Scripta Materialia* 229 (2023): 115368.

64. H.-K. Noh, K.-J. Chang, B. Ryu, and W.-J. Lee, "Electronic Structure of Oxygen-Vacancy Defects in Amorphous In-Ga-Zn-O Semiconductors," *Physical Review B* 84, no. 11 (2011): 115205.

65. R. Izmailov, J. Strand, N. Ronchi, A. Shluger, and V. Afanas'ev, "Electron Emission from Deep Traps in HfO_2 Under Thermal and Optical Excitation," *Physical Review B* 109 (April 2024): 134109.

66. R. A. Izmailov, J. W. Strand, L. Larcher, B. J. O'Sullivan, A. L. Shluger, and V. V. Afanas'ev, "Electron Trapping in Ferroelectric HfO_2," *Physical Review Materials* 5 (2021): 034415.

67. V. Naumann, M. Otto, R. Wehrspohn, M. Werner, and C. Hagendorf, "Interface and Material Characterization of Thin ALD-Al_2O_3 Layers on Crystalline Silicon," *Energy Procedia* 27 (2012): 312–318.

68. R. Tromp, G. W. Rubloff, P. Balk, F. K. LeGoues, and E. J. van Loenen, "High-Temperature SiO_2 Decomposition at the SiO_2/Si Interface," *Physical Review Letters* 55 (1985): 2332–2335.

69. K. Hofmann, G. Rubloff, M. Liehr, and D. Young, "High-Temperature Reaction and Defect Chemistry at the Si/SiO_2 Interface," *Applied Surface Science* 30, no. 1 (1987): 25–31.

70. A. Padovani, D. Gao, A. Shluger, and L. Larcher, "A Microscopic Mechanism of Dielectric Breakdown in SiO_2 Films: An Insight from Multi-Scale Modeling," *Journal of Applied Physics* 121, no. 15 (2017): 155101.

71. J. Strand, P. La Torraca, A. Padovani, L. Larcher, and A. L. Shluger, "Dielectric Breakdown in HfO_2 Dielectrics: Using Multiscale Modeling to Identify the Critical Physical Processes Involved in Oxide Degradation," *Journal of Applied Physics* 131, no. 23 (2022): 234501.

72. R. Nakamura, M. Ishimaru, H. Yasuda, and H. Nakajima, "Atomic Rearrangements in Amorphous Al_2O_3 Under Electron-Beam Irradiation," *Journal of Applied Physics* 113, no. 6 (2013): 064312.

73. A. Zaborowska, A. Kurpaska, M. Clozel, et al., "Absolute Radiation Tolerance of Amorphous Alumina Coatings at Room Temperature," *Ceramics International* 47, no. 24 (2021): 34740–34750.

74. C. Koroni, T. Olsen, J. P. Wharry, and H. Xiong, "Irradiation-Induced Amorphous-to-Crystalline Phase Transformations in Ceramic Materials," *Materials* 15, no. 17 (2022): 5924.